

## Synthetic Unruh effect in cold atoms

Javier Rodríguez-Laguna,<sup>1,2</sup> Leticia Tarruell,<sup>2</sup> Maciej Lewenstein,<sup>2,3</sup> and Alessio Celi<sup>2</sup>

<sup>1</sup>Departamento Física Fundamental, Universidad Nacional de Educación a Distancia (UNED), Madrid, Spain

<sup>2</sup>ICFO-Institut de Ciències Fotòniques, The Barcelona Institute of Science and Technology, 08860 Castelldefels (Barcelona), Spain

<sup>3</sup>ICREA-Institució Catalana de Recerca i Estudis Avançats, Lluís Companys 23, 08010 Barcelona, Spain

(Received 20 July 2016; published 24 January 2017)

We propose to simulate a Dirac field near an event horizon using ultracold atoms in an optical lattice. Such a quantum simulator allows for the observation of the celebrated Unruh effect. Our proposal involves three stages: (1) preparation of the ground state of a massless two-dimensional Dirac field in Minkowski space-time; (2) quench of the optical lattice setup to simulate how an accelerated observer would view that state; (3) measurement of the local quantum fluctuation spectra by one-particle excitation spectroscopy in order to simulate a De Witt detector. According to Unruh's prediction, fluctuations measured in such a way must be thermal. Moreover, following Takagi's inversion theorem, they will obey the Bose-Einstein distribution, which will smoothly transform into the Fermi-Dirac as one of the dimensions of the lattice is reduced.

DOI: [10.1103/PhysRevA.95.013627](https://doi.org/10.1103/PhysRevA.95.013627)

### I. INTRODUCTION

The path towards quantum gravity opened a territory full of surprises: quantum field theory in curved space-time [1]. Bekenstein's phenomenological thermodynamics of black holes [2] received a strong support from Hawking, when he found that a black hole must emit thermal radiation [3]. The discovery hinted that thermal effects might appear without any underlying stochasticity. Fulling, Davies, and Unruh proposed that a similar effect existed in an essentially flat space-time, i.e., Rindler space-time: an accelerated observer through an empty Minkowski space-time will perceive a thermal bath of particles, at a temperature proportional to its acceleration [4–6]. Both phenomena are intimately related: in both cases, an event horizon, which prevents communication between different regions of space-time, is developed. Furthermore, in order to observe Hawking's radiation, one must stay at rest near a black hole, and therefore feel an acceleration. A further surprise was revealed when Takagi studied the relation between dimensionality and the Unruh thermal spectrum [7]. In 3+1 dimensions [(3+1)D], an accelerated detector of bosonic particles in Minkowski space-time will record a Bose-Einstein distribution, and a detector of fermionic particles will find a Fermi-Dirac distribution. But, this is only true if the dimension of space is odd. Otherwise, an apparent *statistics inversion* phenomenon takes place: bosons are detected with a Fermi-Dirac distribution, while fermions are detected with a Bose-Einstein distribution. The Unruh effect is not just an exotic curiosity: it bears a deep relation to entanglement [8] and black-hole thermodynamics, and it plays a central role in Jacobson's derivation of Einstein equations as equations of state for space-times in thermal equilibrium [9]. These results point to a fundamental nature of the Unruh effect as a quantum counterpart of the principle of equivalence, which it corrects [10]. Moreover, the Unruh effect can be regarded as a particular case of *parametric amplification* of the vacuum fluctuations [11], which puts it in the same class of phenomena as the dynamical Casimir effect [12–14]. The latter can be seen as a flat space-time analog of the Hawking effect and connected with the Unruh thermal bath close to the black-hole horizon. The intriguing relation between the Unruh and dynamical

Casimir effects has been also explored in the context of brane physics [15,16].

The fundamental relevance of the Unruh effect provides a strong motivation to measure it and related phenomena in the laboratory [17] (see also [18] for some more recent proposals). Given the difficulty of the task, a different approach has been to develop analog gravity systems where Hawking radiation might show up [19,20]. One of the first ideas [21] was to build a *sonic analog* of a black hole in a moving medium, whose speed of sound replaces the speed of light. If the relative velocity between parts of the propagating medium is larger than the speed of sound, an effective horizon appears. The medium can be either water [22,23] or a Bose-Einstein condensate (BEC) [24–28], which can be employed also to probe the dynamical Casimir effect [29–32]. A specific proposal for measuring the Unruh effect in this setting, using an accelerated impurity as De Witt detector, was proposed in [33] (impurities can be used also as detectors of Casimir forces and quantum friction [34]). Other very interesting approaches are to use a nonlinear optical medium in which a refractive index perturbation moves at high speed [35–39], or to exploit the geometric properties of graphene sheets [40–42]. The use of engineered lattices of superconducting qubits [11] has been already used to probe the dynamical Casimir effect [43] and proposed for Unruh physics.

In this work, we take a different strategy and propose an alternative framework for simulating the Unruh effect, which is based on the *quantum simulation* of Dirac fermions using ultracold fermionic atoms in a two-dimensional (2D) optical lattice [44,45]. The possibility of simulating the Dirac Hamiltonian in certain space-time metrics was recently put forward by some of us, where the information about the metric is encoded in the tunneling terms shaped by the lasers [46]. Building upon that framework, we propose to start the experiment by setting up an optical lattice whose dynamics simulates the massless Dirac Hamiltonian in (2+1)D in Minkowski space-time, where the Fermi velocity, analog to the speed of sound in a BEC, plays the role of the speed of light. By achieving the ground state, we can assume that our quantum state is the Dirac vacuum in Minkowski space-time. Now, we can *quench* the system by suddenly changing the tunneling terms in the lattice to the values corresponding to the Dirac

Hamiltonian in a Rindler metric. In other terms, the same Dirac physics, Minkowski vacuum of Dirac fermions, but viewed by an accelerated observer. Canonical observation of the Unruh effect should be performed now by a local *De Witt detector* [1], a device whose purpose is to couple minimally to the quantum fluctuations of the field and interchange energy [7]. The full spectrum of local fluctuations obtained is predicted to follow both Unruh and Takagi's predictions.

What is special about our approach? Our setup is a quantum simulator, i.e., a *quantum computer of special purpose* [45] that allows for a systematic study of gravitating quantum matter. For instance, within our quantum simulator it is possible to change the Fermi velocity or the shape of the metric. More importantly, it provides a framework for systematically studying quantum many-body systems [47]. Beyond the free fields studied in this work, let us emphasize that the setup we propose for simulating the Unruh effect can be used also for studying interacting fermions in curved space-time, and that it allows for the subtle manipulations needed to simulate experiments in relativistic quantum information [48]. Another parameter which can be easily tuned is the dimensionality of the artificial space-time, thus allowing us to probe the aforementioned inversion theorem of Takagi [7].

The investigation of the Unruh effect bears a strong relation to the study of boundary effects. Indeed, the horizon can be considered as a boundary for fields which are accessible to the accelerated observer. Ensuring that the boundary conditions do not spoil the unitarity of the theory imposes certain conditions on the Hamiltonian [49] which, as we will show, are fulfilled naturally for the Dirac Hamiltonian in Rindler space-time, and provides a procedure to perform the right discretization. Surprisingly, our Hamiltonian has the same form as one of the candidates to solve the Riemann conjecture via the Hilbert-Polya approach,  $H = xp$  [50–53]. In a different line, our model bears relation to the hyperbolically deformed Hamiltonians [54,55] and to the techniques of off-diagonal confinement in optical lattices [56].

As our work is meant to be directed to a wide audience, we try as much as possible to keep it self-contained. In Sec. II we provide a pedagogical overview of the relativistic physics for an accelerated observer, both classical and quantum. Section III introduces the Dirac Hamiltonian in Rindler space-time and discusses its discretization. Readers mainly interested in the proposed quantum simulation of the Unruh effect could go directly to Sec. IV, where we detail our quench strategy, provide numerical simulations of the expected results, and suggest a possible experimental implementation. We finish in Sec. V with conclusions and proposals for further work.

## II. REVIEW OF RINDLER SPACE-TIME AND QFT IN CURVED SPACE-TIME

This section is a review of the physics of an accelerated observer. We will discuss in a pedagogical fashion the basics of the Rindler metric, the thermalization theorem, and the Unruh effect.

### A. Rindler space-time

Let us briefly review Rindler physics, i.e., Minkowski space-time viewed by an accelerated observer [57–59]. Let us

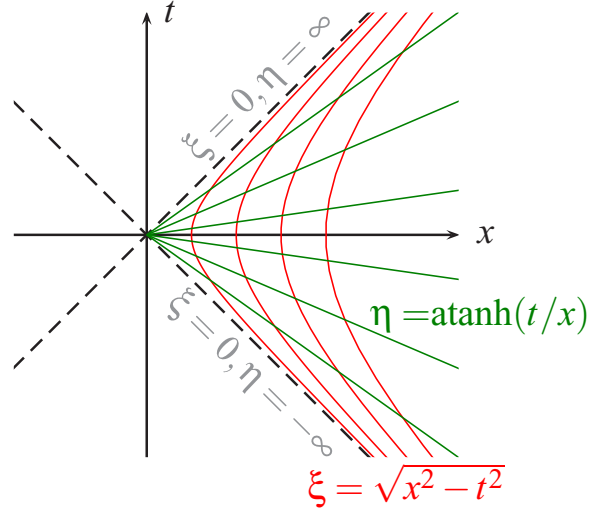


FIG. 1. Rindler coordinates on (1+1)D Minkowski space-time,  $\eta$  (Rindler time) and  $\xi$  (Rindler space). For convenience, the speed of light  $c$  is taken to be 1 and both  $(x, t)$  and  $(\xi, \eta)$  are measured in arbitrary units of length. The Rindler wedge, delimited by dashed lines, is the domain of validity of the coordinate patch. Constant  $\eta$  lines (green) are spacelike, and constant  $\xi$  lines (red) are timelike. For simplicity, we plot the trajectories only in the right wedge,  $x > 0$ , as the ones for the wedge  $x < 0$  can be obtained by reflection around the  $y$  axis. Note that as detailed in Sec. IV, both wedges are realized and are at the same footing in our proposal.

consider an observer moving with constant acceleration  $a = 1$  (for convenience in the following we take the speed of light to be  $c = 1$ ) in the positive  $x$  axis, at rest at  $t = 0$  and  $x = 1$ . Physics seen by this observer is more properly described in a comoving reference frame, obtained by the Fermi-Walker transport procedure. Let  $\eta$  be the comoving time coordinate for this observer, and  $\xi$  the comoving space coordinate. They are called *Rindler coordinates*, and can be found using this transformation (see Fig. 1)

$$\begin{aligned} t &= \xi \sinh \eta, \\ x &= \xi \cosh \eta. \end{aligned} \quad (1)$$

In particular, the considered trajectory corresponds to  $\xi = 1$  for all  $\eta$ . Notice the similarity with polar coordinates, where  $\xi$  plays the role of a radius and  $\eta$  is an angle in hyperbolic geometry. The principle of equivalence states that physics seen by a noninertial observer can be absorbed by a change in her metric. Indeed, in these coordinates, the Minkowski metric becomes

$$ds^2 = -\xi^2 d\eta^2 + d\xi^2 + dy^2 + dz^2, \quad (2)$$

which is known as the Rindler metric. Notice that the Rindler time direction corresponds to a symmetry of the metric, i.e., it constitutes a Killing vector which is inequivalent to the usual Minkowski time direction. In fact, it corresponds to a boost transformation. In the polar coordinates view, it is the generator of hyperbolic rotations. Furthermore, the pole  $\xi = 0$  corresponds to a singularity in the coordinate system because the coefficient of  $d\eta^2$  vanishes. This is the hallmark of an *event horizon*. In fact, one can consider the Rindler metric (2) as a

particular example of *optical metric* where the only nontrivial entry of the metric is  $g_{00}$ , which becomes position dependent. These are called optical metrics because propagation of light along the geodesics is equivalent to “Galilean” propagation in a refractive medium with a position-dependent refractive index  $n(x)$ , which implies the “local” speed of light  $c_{\text{loc}}(x) = 1/n(x)$ . The corresponding optical metric is of the form

$$ds^2 = -c_{\text{loc}}^2(x, y, z)dt^2 + dx^2 + dy^2 + dz^2. \quad (3)$$

For Rindler space-time,  $c_{\text{loc}}^2(\xi) = \xi^2$ . As  $\xi \rightarrow 0$ , the local speed of light vanishes, which implies that signals cannot propagate beyond that point. Thus, space-time is separated into two parts which do not communicate: the two Rindler wedges  $\xi > 0$  and  $\xi < 0$ . It is remarkable that an event horizon can appear even in a flat space-time.

Let us return to the proposed accelerated observer, which in Rindler space-time just sits at rest at  $\xi = 1$ . From her point of view, light moves at her left more slowly than usually, and faster at her right. Near the horizon,  $\xi = 0$ , light moves more and more slowly, coming to stop at  $\xi = 0$ , i.e., its local speed of light is zero (while the actual speed of light stays obviously constant to 1). Let us now consider objects which are static with respect to the accelerated observer, i.e., objects at rest in Rindler space-time at different values of  $\xi$ . Tracing back their trajectories to Minkowski space-time, it can be checked that they correspond also to accelerated trajectories, with acceleration  $a(\xi) = 1/\xi$ . This implies that, in order to keep pace with an observer with acceleration  $a$  in front of you, you must accelerate faster than that [58]. This result is known as *Bell’s spaceship paradox*.

### B. Thermalization theorem

The interplay between thermodynamics and general relativity gives rise to surprising properties. Let us restrict ourselves to space-times which contain a timelike Killing vector, i.e., space-times whose metric can be said to be time invariant, where we have a well-defined concept of energy. In that case, *Tolman-Ehrenfest’s theorem* [7,60] states that for any field in thermal equilibrium within a stationary curved space-time, the product of the local temperature and the modulus of the local timelike Killing vector is constant,  $T g_{00}^{1/2} = \text{const}$ . There is a simple way to visualize this result. Photons emitted at one point  $P$  in space with frequency  $\nu$  will reach another point in  $P'$  with a red-shifted frequency  $\nu(P') = \nu(P)\sqrt{g_{00}(P)/g_{00}(P')}$ . Thus, the same factor should be applied to energies and to temperatures. Thus, in Rindler space-time, temperature at any point is inversely proportional to the distance to the horizon. Or, in other words, it is proportional to the acceleration of an observer stationary at that point. Notice that this does not entail a nonzero temperature. The theorem still holds if the temperature is zero everywhere.

But, the biggest surprises show up when we introduce quantum mechanics [1]. Let us consider a free-fermionic field in Minkowski space-time, with Hamiltonian  $H_M$ , described in terms of local creation operators  $c_x^\dagger$ . The physical vacuum is the ground state of its Hamiltonian  $|0_M\rangle$ , and it does not correspond to the Fock vacuum  $|\Omega\rangle$ , which is defined by  $c_x|\Omega\rangle = 0$  for all  $x$ . In the physical vacuum, all the

negative-energy single-particle modes will be occupied

$$|0_M\rangle = \prod_{\omega_k^M < 0} b_k^\dagger |\Omega\rangle, \quad (4)$$

where  $b_k^\dagger$  creates the  $k$ th mode, and  $\hbar\omega_k^M$  is its energy. According to the usual convention,  $b_k^\dagger$  creates a particle if  $\omega_k^M > 0$  and an antiparticle if  $\omega_k^M < 0$ . Therefore, the physical vacuum is built by occupying all the antiparticle states, and none of the particle ones.

Let us now consider an accelerated observer moving through this vacuum. She will see physics displayed not on Minkowski space-time, but on a Rindler metric (2). Let  $H_R$  be the appropriate Hamiltonian operator, which is also a free-fermionic Hamiltonian. Its single-particle modes are known as the Rindler modes  $d_q^\dagger$ . They have energies  $\hbar\omega_q^R$  and are solutions to the wave equation in the Rindler metric (here the index  $q$  labels the eigenstates, but does not correspond to momentum in the acceleration direction since translational invariance is broken). The ground state of  $H_R$  is

$$|0_R\rangle = \prod_{\omega_q^R < 0} d_q^\dagger |\Omega\rangle. \quad (5)$$

Again, the Rindler modes will qualify either as particles, if  $\omega_q^R > 0$ , or antiparticles if  $\omega_q^R < 0$ . The pure state  $|0_M\rangle$  does not need to be an eigenstate of  $H_R$ , much less its ground state. From the point of view of the accelerated observer, who measures energies with  $H_R$ ,  $|0_M\rangle$  is not the true vacuum any more. How does this state look like to her? It is crucial to realize that the Rindler metric has a horizon, which separates space into two parts which cannot communicate. Thus, she will not detect  $|0_M\rangle$ , but the *reduced density matrix* which results from tracing out the hidden part

$$\rho_R = \text{Tr}_L |0_M\rangle \langle 0_M|, \quad (6)$$

where  $\text{Tr}_L$  means a trace over the left-out degrees of freedom. A reduced density matrix can always be formally written as a thermal state

$$\rho_R = \exp(-H_E), \quad (7)$$

where  $H_E$  is called the entanglement Hamiltonian [8,61]. Since the Minkowski vacuum (4) is a Slater determinant, we can use Wick’s theorem in reverse to prove that the entanglement Hamiltonian must be a free-fermionic Hamiltonian [62]. In other terms, the accelerated observer will see a thermal state of free particles. The Minkowski vacuum is invariant under Lorentz boosts, which correspond to time translations in Rindler space-time. For  $\rho_R$ , this property implies

$$0 = \dot{\rho}_R = -\frac{i}{\hbar}[\rho_R, H_R]. \quad (8)$$

Thus,  $[H_E, H_R] = 0$ , i.e., the entanglement Hamiltonian and the Rindler Hamiltonian must commute. In fact, they can be nontrivially proved to be proportional, and the constant of proportionality can be read as an inverse temperature

$$\rho_R = \exp\left(-\frac{H_R}{k_B T_U}\right), \quad (9)$$

where

$$k_B T_U = \frac{\hbar a}{2\pi}. \quad (10)$$

Here,  $T_U$  is known as the *Unruh temperature* and this result, which is far more general than the particular case studied here, is the *thermalization theorem* [7]. Thus, the Unruh temperature does not appear because of any underlying stochasticity. The loss of information which gives rise to the thermal effect is related to the presence of the horizon. An important consequence of thermalization theorem is that Minkowski vacuum *appears to be stationary to an accelerated observer*. Indeed, while Minkowski vacuum is clearly not an eigenstate of Dirac Hamiltonian in Rindler space-time and, thus, evolves nontrivially in Rindler time, *what an accelerated observer detects is invariant under such time evolution* as the thermal state is a diagonal density matrix in the Rindler eigenbases. This observation is crucial in our proposal for simulating the Unruh effect with ultracold atoms (see Sec. IV).

### C. Unruh effect

Let us consider the canonical transformation between Minkowski ( $b_k^\dagger$ ) and Rindler modes ( $d_q^\dagger$ )

$$d_q^\dagger = \sum_k U_{qk} b_k^\dagger. \quad (11)$$

This is a Bogoliubov transformation in disguise because a positive-energy Rindler mode (particle) requires both positive and negative Minkowski modes for its expansion (particle and antiparticle). In fact, as the acceleration is position dependent, the relevant Bogoliubov transformation has to be defined locally. In the continuous limit, the global Bogoliubov transformation (11) is even ill defined as the eigenstates are not normalizable. In order to properly define it, we have to consider normalized states [7], for instance, wave packets centered around a generic point  $\mathbf{r}$ . On physical terms, this means that we can associate a well-defined acceleration to the Rindler wave packet. For practical purposes, the wave-packet normalization is equivalent to restricting the scalar product of the unnormalized modes to a small region  $D_{\mathbf{r},\epsilon}$  such that  $|\mathbf{r}' - \mathbf{r}| \leq \epsilon$  of space around  $\mathbf{r}$ . With this definition, the occupation of each Rindler mode on the Minkowski ground state is given by

$$n_{q,\mathbf{r}} \equiv \int_{D_{\mathbf{r},\epsilon}} \langle 0_M | d_q^\dagger | \mathbf{r}' \rangle \langle \mathbf{r}' | d_q | 0_M \rangle = \sum_{\omega_k^M < 0} |\tilde{U}_{qk}(\mathbf{r})|^2, \quad (12)$$

and the thermalization theorem ensures that

$$n_{q,\mathbf{r}} = \frac{1}{\exp[\hbar\omega_q^R/k_B T_U(\mathbf{r})] + 1}, \quad (13)$$

with  $k_B T_U(\mathbf{r}) = \frac{\hbar}{2\pi x}$  according to Eq. (10), where  $x$  is the spatial distance of the point  $\mathbf{r}$  from the horizon.

But, the *Unruh effect* goes beyond the thermalization theorem because it is defined *operationally*, in terms of what a local observer can measure. The so-called *De Witt* detector [1,7] is a device carried along with the observer, which couples minimally to the fermionic field at a spatial point  $\mathbf{r}$ , and can emit and absorb particles. Under a large variety of circumstances it can be proved that the probability amplitude

of absorption and emission is given solely by the *Wightman function*

$$G(t) \equiv \langle 0_M | c_{x(t)}^\dagger(t) c_{x(0)}(0) | 0_M \rangle. \quad (14)$$

Here,  $x(t)$  is the trajectory for the observer (for simplicity we consider trajectories parallel to the  $x$  axis and we omit remaining constant spatial coordinates) and  $c_x^\dagger(t)$  is the creation operator for a fermion at event  $(x,t)$ . The Fourier transform of  $G(t)$ ,  $G(\omega)$  is the *detector response function*, which should be experimentally accessible, as we will discuss later.

The formula (14) makes equal sense in Minkowski or in Rindler space-times, if we are allowed to abuse notation and let  $x$  and  $t$  denote the coordinates in both. In Rindler space-time, the trajectory of an accelerated observer will be just a constant  $x(t) = x_0$ . Let us define two different basis changes, from Rindler space-localized states to Rindler and Minkowski modes, respectively. At time  $t = 0$ , if  $c_x^\dagger$  creates a particle at point  $x$ , we have

$$\begin{aligned} b_k^\dagger &= \sum_x M_{kx} c_x^\dagger, \\ d_q^\dagger &= \sum_x R_{qx} c_x^\dagger, \end{aligned} \quad (15)$$

where the unitary matrices  $M_{kx}$  and  $R_{qx}$  are the single-particle wave functions of Minkowski and Rindler modes, respectively, and determine the unitary transformation  $U_{qk}$  in (11),  $U_{qk} = \sum_x R_{qx} \bar{M}_{kx}$ . Here and in the following by the bar we denote the complex conjugate of the matrix elements. So, we get

$$\begin{aligned} G_{x_0}(\omega) &\equiv \int dt e^{-i\omega t} \langle 0_M | c_{x_0}^\dagger(t) c_{x_0}(0) | 0_M \rangle \\ &= \sum_{q,q'} \delta(\omega - \omega_q^R) \bar{R}_{qx_0} R_{q'x_0} \sum_{\omega_k^M < 0} \bar{U}_{qk} U_{q'k}. \end{aligned} \quad (16)$$

Thus, the detector response function is strongly dependent on the form of the Rindler and Minkowski modes, through  $U$  and  $R$ .

Going beyond the thermalization theorem, Unruh predicted that the distribution function  $G(\omega)$  will be *thermal*. But, a surprise is hiding behind Eq. (16) due to the spatial dependence of the Rindler and Minkowski modes. If the dimension of space is *odd*, then the response function of a fermionic field will follow the Fermi-Dirac distribution function, as one would expect. But if the dimension of space is *even*,  $G_{x_0}(\omega)$  will follow a Bose-Einstein distribution. The opposite is true for a free bosonic field. This fact, known as Takagi's inversion theorem [7], stems from dimensional effects in wave propagation, analogous to those observed for light propagating radially. In odd dimension, the Huygens principle holds, and a pointlike perturbation after a time  $t$  is concentrated in a spherical shell of radius  $vt$ , where  $v$  is the propagation velocity. In even dimension, however, not all the scattered waves propagate at the same  $v$ , the Huygens' principle does not hold and the perturbation becomes radially spread with time.

Alternative physical meanings of the detector response function (16) are worth mentioning. The first is a measure of quantum fluctuations:  $G_{x_0}(\omega)$  is the power spectrum of the

quantum noise [63]. The second is related to the dynamical Casimir effect. Let us consider a physical plane in space, whose interaction with our fermionic field can be expressed as a Dirichlet boundary condition. Now, let us move this plane with constant acceleration  $a$ . Then, the stress-energy tensor at any point will depend on its current distance to the plane. In fact, it can be proved [7,64] that the limit  $a \rightarrow \infty$  can be made meaningful, thus providing a well-defined stress-energy tensor for the Rindler vacuum, which induces quantum fluctuations that are probed by expression (16).

### III. DIRAC FERMIONS IN A RINDLER LATTICE

In this section, we describe the behavior of Dirac fermions in Rindler space-time for one and two spatial dimensions. In particular, we explicitly construct the corresponding Hamiltonian in a square lattice. Indeed, since the Rindler metric has a timelike Killing vector field, we can use a Hamiltonian formalism and discretize it to get a simple tunneling model. The resulting model bears a surprising resemblance to the  $xp$  Hamiltonian used in the Hilbert-Polya approach to proving the Riemann conjecture. This point is further detailed in the Appendix.

#### A. Dirac Hamiltonian in Rindler space-time

Let us consider a relativistic massless fermionic field in two dimensions, governed by the Dirac equation in Minkowski space-time

$$\gamma^a \partial_a \psi = 0, \quad (17)$$

where the  $\gamma^a$  are a representation of the Clifford algebra,  $\{\gamma^a, \gamma^b\} = 2\eta^{ab}$ , where  $\eta_{ab} = \text{Diag}(-1, 1, 1)$  is the Minkowski metric and  $a, b = 0, 1, 2$ . In (17), as well as in the rest of the section, sums over repeated indices are left implicit according to Einstein's convention. As it stands, the equation is manifestly Lorentz covariant. Let us shift to a Hamiltonian view, which is more convenient for simulation. In other words, we single out the time derivative

$$i\partial_0 \psi = \mathcal{H}\psi = -i\gamma_0 \gamma^j \partial_j \psi, \quad j = 1, 2. \quad (18)$$

Let us make the following choice for the  $\gamma_a$  matrices in two dimensions,  $-\gamma_2 = \sigma_x$ ,  $\gamma_1 = \sigma_y$ ,  $\gamma_0 = i\sigma_z$ . We obtain

$$i\partial_t \psi = -i(\partial_x \sigma_x + \partial_y \sigma_y) \psi. \quad (19)$$

Equation (17) can be formulated on a general (curved) background metric  $g_{\mu\nu}$  as well. For spinor systems it is very convenient to introduce the *vielbein*, which is a set of vectors defined on the tangent manifold  $e_\mu^a(x)$ , such that  $g_{\mu\nu}(x) = e_\mu^a(x) e_\nu^b(x) \eta_{ab}$ . The parallel transport for the vielbein vectors defines the *spin connection*  $w_\mu^{ab}$ , and allows a compact expression for the covariant derivative of a spinorial field [58]

$$\partial_\mu \psi \rightarrow D_\mu \psi \equiv \left( \partial_\mu + \frac{1}{4} w_\mu^{ab} \gamma_{ab} \right) \psi, \quad (20)$$

where  $\gamma_{ab} \equiv \frac{1}{2}[\gamma_a, \gamma_b]$ . By making use of it, the Dirac equation reads as

$$\gamma^\mu D_\mu \psi = 0, \quad (21)$$

where the *curved* gamma matrices  $\gamma_\mu$  are defined by  $\gamma_\mu = \gamma_a e_\mu^a$ , and the curved indices  $\mu = t, x, y$  are lowered and raised by contracting with the metric  $g_{\mu\nu}$  and its inverse  $g^{\mu\nu}$ . When we single out the time derivative, we obtain again a Schrödinger equation of the form

$$i\partial_t \psi = -i\gamma_t (\gamma^j \partial_j + \frac{1}{4} \gamma^j w_j^{ab} \gamma_{ab} + \frac{1}{4} \gamma^t w_t^{ab} \gamma_{ab}) \psi, \quad (22)$$

where  $j = x, y$ .

Let us now consider the specific case of the 2D Rindler metric (2)  $ds^2 = -x^2 dt^2 + dx^2 + dy^2$ . The only nonvanishing element of the spin connection is  $w_t^{01} = x/|x|$ . With the aforementioned choice for the  $\gamma_a$  matrices, we get

$$i\partial_t \psi = -i \left[ \left( |x| \partial_x + \frac{1}{2} \frac{x}{|x|} \right) \sigma_x + |x| \partial_y \sigma_y \right] \psi. \quad (23)$$

Thus, the Hamiltonian density becomes

$$\mathcal{H}_R = -i \left[ \left( |x| \partial_x + \frac{1}{2} \frac{x}{|x|} \right) \sigma_x + |x| \partial_y \sigma_y \right], \quad (24)$$

which is the single-particle Rindler Hamiltonian. Its second-quantized form is simply

$$H_R = \int dx dy \bar{\psi}^\dagger \mathcal{H}_R \psi. \quad (25)$$

The same expression can obviously be derived by taking the Legendre transformation of the Dirac Lagrangian in Rindler space-time.

In intuitive terms, the  $|x|$  term is related to the volume form  $\sqrt{-g} = |x|$ . The  $\frac{1}{2}$  term comes for the covariant derivative and it is essential to ensure the Hermiticity of  $H_R$ . Indeed, this factor cancels the so-called *deficiency indices* [49,65], i.e., allows us to treat the horizon at  $x = 0$  as a boundary, ensuring that any boundary condition can be imposed while respecting self-adjointness of the Hamiltonian.

This property is more evident once (25) is cast in symmetric fashion, i.e., the spatial derivatives act symmetrically both on  $\psi$  and  $\psi^\dagger$ :

$$\begin{aligned} H_R &= \frac{1}{2} \int dx dy (\mathcal{H}\psi)^\dagger \psi + \frac{1}{2} \int dx dy \psi^\dagger \mathcal{H}\psi \\ &= \frac{i}{2} \int dx dy |x| [(\partial_x \psi^\dagger) \sigma_x \psi + (\partial_y \psi^\dagger) \sigma_y \psi \\ &\quad - \psi^\dagger \sigma_x \partial_x \psi - \psi^\dagger \sigma_y \partial_y \psi]. \end{aligned} \quad (26)$$

In this form, the propagation in Rindler metric is sensitive only to the overall scale factor which determines a Fermi velocity that changes linearly along the  $x$  direction.

It is worth noticing that the equivalent symmetric formulation of single-particle Hamiltonian (24) is

$$\mathcal{H}_R = \sqrt{x} \not{p} \sqrt{x}, \quad (27)$$

which is also manifestly Hermitian. It will be further discussed in the Appendix, in relation with the Riemann conjecture.

#### B. Discretizing the Rindler Hamiltonian

The Minkowski and Rindler Dirac Hamiltonians in one and two spatial dimensions can be suitably discretized on the lattice [46]. As shown in detail in the Appendix, Sec. A 1, a

convenient way of doing this is to consider a 1D chain or a 2D square lattice with noninteracting spinless fermions

$$H = - \sum_{\langle \mathbf{r}, \mathbf{r}' \rangle} t_{\mathbf{r}\mathbf{r}'} c_{\mathbf{r}}^\dagger c_{\mathbf{r}'} + \text{H.c.}, \quad (28)$$

where the sum runs over all pairs of nearest-neighbors sites  $\mathbf{r}, \mathbf{r}'$ . Since the 1D Dirac models can be realized as a slice along  $x$  (defined as the direction perpendicular to the Rindler horizon) of the 2D Dirac ones, we focus on the latter case. Hamiltonian (28) can represent the dynamics of each of the chiral components of the Minkowski Dirac Hamiltonian if the tunneling terms  $t_{\mathbf{r}\mathbf{r}'}$  have all the same modulus and the sum of their phases around each plaquette is  $\pi$ . This corresponds to the well-known  $\pi$ -flux Hamiltonian [66–68]. All possible choices of phases respecting the  $\pi$ -flux condition are equivalent, as they are related by gauge transformations. We will focus on the one corresponding to the symmetry gauge for the synthetic gauge field associated to the phases. Precisely,

$$H_M = - \sum_{m,n} t_0 (e^{i\frac{\pi}{2}(m-n)} c_{m+1,n}^\dagger + e^{i\frac{\pi}{2}(m-n)} c_{m,n+1}^\dagger) c_{m,n} + \text{H.c.}, \quad (29)$$

where we adopt Cartesian coordinates to parametrize the lattice  $\mathbf{r} = (m d, n d)$  and denote with  $d$  the lattice spacing.

The discretized version of the Rindler Dirac Hamiltonian (26) can also be chosen to be of the form (28), but with spatially modulated tunnelings  $t_{\mathbf{r}\mathbf{r}'}$ . Each tunneling rate has to be proportional to the average  $x$  coordinate of each link, which represents the distance from the horizon. We place the horizon at  $x = 0$  accordingly to the coordinates chosen in (3). The tunneling phases have to satisfy the same  $\pi$ -flux condition as for the Dirac Hamiltonian in Minkowski space. For the symmetric gauge choice of (29) we have

$$H_R = - \sum_{m,n} t'_0 [(m + \frac{1}{2}) e^{i\frac{\pi}{2}(m-n)} c_{m+1,n}^\dagger + m e^{i\frac{\pi}{2}(m-n)} c_{m,n+1}^\dagger] \times c_{m,n} + \text{H.c.} \quad (30)$$

The numerical simulation and the experimental implementation in optical lattices of the Hamiltonians (29) and (30) will be discussed in the next section. We would like to remark here that in principle any other lattice realization of the Dirac Hamiltonian like the ones in bichromatic [69], hexagonal [70,71], and brick-wall lattices [44], which do not involve artificial gauge fields, can be considered and deformed by shaping the tunneling term to reproduce the Dirac Hamiltonian in Rindler space-time. Other artificial lattice Dirac systems such as nanopatterned 2D electron gases, photonic crystals, microwave lattices [72], or polaritons [73] could also be used. Since the Unruh effect is a single-particle and purely kinematic effect, it could be studied using both bosonic and fermionic systems. The latter offers a simple route to explore the relativistic (linear dispersion relation) regime, as detailed in the next section.

#### IV. SIMULATING THE UNRUH EFFECT WITH COLD ATOMS

In this section, we present our proposal to study the Unruh effect for Dirac fermions in an optical lattice, in one and two

spatial dimensions. The crucial idea behind our proposal is that all measurements made by an accelerated observer on the Minkowski vacuum of the Dirac field can be simulated by *quenching* the Dirac Hamiltonian from the one in Minkowski space-time to the one in Rindler space-time, which amounts to quench the tunneling amplitudes from constant to properly position-dependent values. As a by far nontrivial consequence of thermalization theorem (cf. Sec. II B), the Minkowski vacuum will now be seen as a thermal state in Rindler, which we will subsequently probe with a suitable analog of De Witt detectors, yielding the local fluctuation spectrum predicted by the Unruh effect. As a thermal state corresponds only to populations of Rindler modes, the Minkowski vacuum is stationary, that is to say that is invariant under time translations in Rindler space-time (this property is not so surprising because Rindler time translations correspond to Lorentz boosts in the original Minkowski coordinates).

We start by providing an overview of the experimental procedure. Our scheme relies crucially on one-particle excitation spectroscopy, which we discuss in detail. The robustness of our scheme is then validated by performing a numerical simulation of the response function in realistic experimental conditions. We conclude by proposing an experimental implementation of the protocol which is accessible using state-of-the-art techniques.

##### A. Strategy

As explained in Sec. IIC, the observation of the Unruh effect requires a measurement of the Wightman two-point correlation function in the frequency domain (14) for an accelerated observer in the Minkowski vacuum. In other terms, we have to measure the Fourier transform of two-point correlations in time. For a Dirac system as the one we consider, the Minkowski vacuum is the Fermi sea, and what needs to be measured is the overlap between the state corresponding to a one-hole excitation at different times. Furthermore, this one-hole excitation must follow an accelerated trajectory.

Traditionally, an accelerated observer is considered in order to observe the Unruh effect, with the Minkowski vacuum at rest and the one-hole excitation moving. For instance, this is the approach considered in [33], where the one-hole excitation is created by the coupling to an impurity. However, due to the equivalence principle, the measurement can actually be done in any reference frame. We choose to perform it in the rest frame of the observer and the one-hole excitation. There, the time evolution is governed by the Dirac Hamiltonian in Rindler space-time [Eq. (24)], and the response function is simply the overlap between the one-hole excitation at rest at different times. The measurement of the Wightman spectral function can then be interpreted as the creation of a one-hole excitation at a fixed location  $x_0$  in the Fermi sea, the evolution of this state with the Dirac Hamiltonian in Rindler space-time for a time  $t$ , and the creation of a particle at  $x_0$ . This is exactly what one-particle excitation spectroscopy, a standard technique in cold atom experiments, determines [74].

Thus, our protocol to observe the Unruh effect consists of three steps:

(1) *Preparation of the Minkowski vacuum* by achieving the ground state of the Dirac Hamiltonian with a uniform Fermi velocity (Dirac Hamiltonian in Minkowski space-time).

(2) *Quench to an accelerated frame* governed by the Dirac Hamiltonian with a spatially dependent Fermi velocity (Dirac Hamiltonian in Rindler space-time). The quench introduces an event horizon in the middle of the gas, effectively disconnecting it in two halves.

(3) *Measurement of the Wightman function* in the accelerated (Rindler) frame using local one-particle excitation spectroscopy at point  $x_0$ .

The first two steps provide a convenient method for preparing the Minkowski vacuum as the ground state of a Hamiltonian which can be easily implemented experimentally, and for making it evolve into an accelerated (Rindler) frame. The third step, local one-particle excitation spectroscopy, is the crucial ingredient of our proposal. It creates a one-hole excitation in the gas, whose dynamics in the accelerated (Rindler) frame produces the Bogoliubov transformation (11). And it is this transformation which is responsible for the thermalization theorem and the Unruh effect. Given its importance, we describe it in detail in the next section.

### B. Measurement of the Wightman function

Our proposal for observing the Unruh effect relies on the use of one-particle excitation spectroscopy for measuring the Wightman function. This technique consists in transferring a fraction of atoms of the gas to an auxiliary energy band which is initially unoccupied and has a considerably smaller bandwidth, so that it can be neglected. The process requires a field coupling both bands, and can be implemented in a variety of fashions (radio-frequency, one-photon, or two-photon laser transitions) depending on the atomic species chosen. In our case, we require the process to be local since the Wightman function is defined locally (at point  $x_0$ ) and the Unruh temperature varies as a function of the distance to the horizon.

If we consider the ensemble of the two bands as an effective two-level system, the effect of the coupling can be modeled in the interaction picture as

$$W_{x_0}(t) = W_0[e^{i\omega t} b_{x_0}^\dagger c_{x_0}(t) + e^{-i\omega t} c_{x_0}^\dagger(t) b_{x_0}], \quad (31)$$

where  $\omega$  represents the detuning between the frequency of the field and the energy of the auxiliary band where the operator  $b_{x_0}^\dagger$  ( $b_{x_0}$ ) creates (destroys) an atom, and we assume an integration over all momenta. Since the measurement is performed after the quench, the operator  $c_{x_0}^\dagger(t)$  [ $c_{x_0}(t)$ ] evolves with the Rindler Hamiltonian.

Now, let us compute the occupation of the auxiliary band at a later time. As it is highly excited, we can assume it to be initially empty. The initial state is thus

$$|\Phi\rangle_0 = |\Phi(t=0)\rangle = |0\rangle_b |\Omega\rangle. \quad (32)$$

Taking a sufficiently small coupling  $W_0$  allows us to treat (31) at first order in perturbation theory. We find

$$|\Phi(t)\rangle \sim |0\rangle_b |\Omega\rangle + W_0 \int_0^t dt' e^{i\omega t'} b_{x_0}^\dagger |0\rangle_b c_{x_0}(t') |\Omega\rangle. \quad (33)$$

Then, the occupation  $N_b$  of the auxiliary state for  $t \gg 1/\omega$  is

$$\begin{aligned} N_b &= \langle \Phi(t) | b_{x_0}^\dagger b_{x_0} | \Phi(t) \rangle \\ &= W_0^2 \int_0^t \int_0^t dt' dt'' e^{i\omega(t'-t'')} \langle \Omega | c_{x_0}(t'') c_{x_0}(t') | \Omega \rangle \\ &\propto \int_{-t}^t e^{i\omega t'} \langle \Omega | c_{x_0}(t') c_{x_0}(0) | \Omega \rangle \propto G(\omega), \end{aligned} \quad (34)$$

where we have used translation invariance in time. The calculation above not only demonstrates that local one-particle excitation spectroscopy measures the Wightman spectral function. It also clearly shows that it is the time evolution under the Rindler Hamiltonian which is responsible for the observed thermal response. We have calculated the occupation  $N_b$  assuming that the pulse started at  $t = 0$ , i.e., immediately after the quench (we have used the original Minkowski vacuum to start with). However, the integral (34) depends only on the duration of the pulse, and not on the actual moment at which the pulse starts. This is an experimental manifestation of the stationary of Minkowski vacuum in Rindler space-time and of the time invariance of the associated populations as Rindler particles.

### C. Validity range of the scheme

Let us now discuss in detail the range of validity of our approach and review some possible limitations. In our scheme, we do not implement the Dirac Hamiltonian (both in Minkowski and Rindler space-times) in the continuum, but only a lattice version of it. This introduces a characteristic length scale in the system, the lattice spacing, and an associated UV energy cutoff. Measurements of the Wightman function below this length scale are not meaningful. However, the finite spatial resolution that one-particle excitation spectroscopy will have in the experiment naturally smears out these discretization artifacts. We will show below that a measurement of the response function convolved over two lattice sites is sufficient to suppress most of them. Another consequence of implementing the Dirac Hamiltonian in an optical lattice is that the relativistic dispersion relation only holds in a certain range of energies, in the vicinity of the Dirac points. Thus, the measurements must be restricted to this energy range, which is given by the local tunneling rate. This limitation is common to other proposals for simulating relativistic effects with cold atoms. For instance, using the Bogoliubov excitations of a Bose-Einstein condensate as relativistic particles is only valid in the phononlike regime of the Bogoliubov dispersion relation, and breaks down away from it.

Our protocol relies on a change of reference frame, from a rest frame to an accelerated one. This step is done by quenching the Hamiltonian from Minkowski to Rindler space-time. The change of reference frame should be instantaneous, an approximation which is valid if the quench time is much shorter than the smallest characteristic time scale of the system given by the inverse of the largest tunneling rate. We will see in Sec. IV E that experimentally this is a reasonable assumption. The main effect of the quench is to introduce an artificial horizon in the middle of the lattice that effectively disconnects the left and right halves. Placing the horizon exactly in the

middle of the system is important to minimize the distortions induced by the finite system size. Finally, let us remark that quenching the Hamiltonian of a quantum system normally triggers a temporal evolution of its initial state. In our case, however, as we have observed at the end of Sec. II B and further argued in this section, the Minkowski vacuum looks stationary to the accelerated observer and this dynamics is absent. Indeed, the Rindler Hamiltonian is proportional to the entanglement Hamiltonian of both halves of the system (7). Thus, the density matrices of both halves are time invariant as they are diagonal and depend only on the populations.

The Unruh effect implies that measurements of the Wightman function at different distances from the horizon, and thus different accelerations, will yield different values of the Unruh temperature. In order to compare these measurements, the rates should be measured with respect to the proper time  $\tau$ . For the Rindler metric [Eq. (3)],  $\tau = \xi t$  with  $\xi \propto |x|$ . Thus, frequencies must be scaled by  $1/\xi$ . At the same time, the Fourier transformation of the Wightman function  $G(t)$  has to be performed with respect to the proper time. In the frequency domain, it is then given by  $\xi G(\omega/\xi)$ .

Finally, up to now we have been assuming that the Minkowski vacuum can be exactly realized in the experiment. Or, in other terms, that it is possible to prepare perfectly the ground state of the Dirac Hamiltonian in the homogeneous tunneling lattice at half-filling (exactly up to the Dirac points). In real experiments, however, the actual temperature of the fermionic gas will not be zero but rather on the order of the tunneling rate. We will show that the signatures of the Unruh effect can still be appreciated when starting with a finite-temperature sample.

#### D. Numerical simulations

In order to validate our scheme and address the effects presented above, we have performed numerical simulations, which we present in this section. The calculations have been done using the  $\pi$ -flux realizations of the Dirac Hamiltonian [Eqs. (29) and (30)] in one and two spatial dimensions. In both cases we have simulated numerically the complete scheme, starting with an initial state in Minkowski space-time, assuming an instantaneous quench, and computing then the Wightman response function as will be measured by one-particle excitation spectroscopy [see Eq. (13)].

In the calculations we fix the system sizes  $L_x$ ,  $L_y$ . The natural energy scale of the system is the bandwidth of the Dirac Hamiltonian in Minkowski space-time [proportional to the tunneling strength  $t_0$  in (29)]. Therefore, all energies (i.e., frequencies and temperatures) are measured in units of  $t_0$ . The amplitude  $t'_0$  that characterizes the tunneling strength of the Dirac Hamiltonian in Rindler space-time (30) is in principle arbitrary due to the overall scale invariance of the Rindler space. We choose it so that the maximal tunneling rate is equal to the Minkowski value  $t'_0 = 2t_0/L_x$ . The lattice spacing is fixed as  $d = 1$  and we attach  $(x, y) = (m, n)$  coordinates to each site in a symmetric way with respect to the horizon, i.e., the  $x = 0$  line. Thus, while  $n$  always runs over integers,  $n = 1, 2, \dots, L_y$ ,  $m$  runs over integers for  $L_x = 2N + 1$  odd,  $m = -N, -N + 1, \dots, N$ , and over half-integers for  $L_x = 2N$  even,  $m = -N + 1/2, -N + 3/2, \dots, N - 1/2$ . Note that

fixing the horizon exactly in the middle of the gas is important to minimize the distortions introduced by the finite size of the system.

As we mentioned in the previous section, in a discrete realization of the Dirac Hamiltonian only measurements performed at length scales above the lattice spacing  $d$  are meaningful. The finite spatial resolution of the measurements will automatically perform the required coarse graining. We simulate it numerically by considering a convolution of the Wightman function (16) with a Gaussian of standard deviation corresponding to two lattice sites along the  $x$  direction. The raw data obtained before the convolution, and further details concerning it are included in the Appendix, Sec. A 3.

The frequency dependence of the response is evaluated at five different positions, at linearly increasing distances from the horizon. The top panel of Fig. 2(a) shows the convoluted results obtained for a 1D system of size  $L_x = 500$ . The tallest (red) curve is the closest to the horizon, and the lowest (blue) one is the most distant. For frequencies close to zero (i.e., the Fermi energy), the response functions all have a behavior resembling a Fermi-Dirac distribution, with strong lattice artifacts at large negative frequencies.

In order to compare the different results, we rescale the curves with respect to the proper time  $\tau$ . The proper frequency is then  $\omega/\xi$ , and the proper rate of detection is  $\xi G(\omega/\xi)$ . For our choice of units  $t_0 = d = 1 = \frac{L_x}{2} t'_0$ ,  $\xi = 2x/L_x$ . Thus,  $\xi = 0$  corresponds to the horizon and  $\xi = 1$  to the edge of the system. Figure 2(b) presents the same curves as Fig. 2(a), but in rescaled units. For frequencies close to  $\omega = 0$ , they reproduce Fermi-Dirac distributions whose temperature increases as we approach the horizon. The distributions are *not* normalized since they are defined up to a global constant.

Notice that in Fig. 2 we have restricted the displayed frequency range to the regime where the energies are lower than the local tunneling range  $|\omega| < |t(x)|$  since it is only there that the dispersion relation remains linear and the description of the particles in terms of Dirac fermions is valid. In rescaled units, this condition becomes  $|\omega/\xi| < 1$ . In the following, we will restrict ourselves to this frequency range.

Figure 3 shows the corresponding results for a 2D system, which differs strongly from its 1D counterpart as predicted by Takagi's inversion theorem. Figure 3(a) shows the rescaled response function for a  $100 \times 100$  lattice, measuring at linearly increasing positions from the horizon as in the 1D case. The displayed curves include the spatial Gaussian convolution, along with an energy coarse graining  $\Delta\omega = 0.2$ . The latter simulates the finite-energy resolution of the measurement, limited by the finite system size. The raw data, prior to convolution and coarse graining, are presented in the Appendix, Sec. A 3. As predicted by Takagi, the results are now similar to a Bose-Einstein distribution.

Finally, in Fig. 3(b) we study the transition between 1D and 2D, by showing the rescaled response functions for a set of lattices with dimensions  $100 \times 1$  (red),  $100 \times 2$ ,  $100 \times 4$ , and  $100 \times 8$  (black), always measured at a point 25 lattice sites away from the horizon. Notice that the Fermi-Dirac distribution disappears very fast when we increase the transverse dimension  $L_y$ .

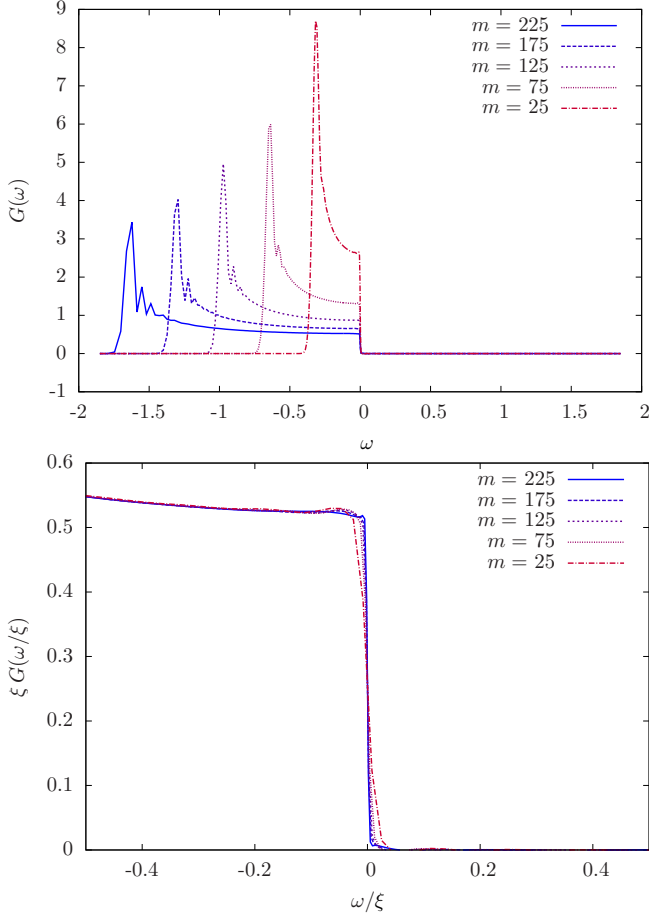


FIG. 2. (a) Wightman response function in the frequency domain for a 1D system of size  $L_x = 500$  after the quench. The frequency  $\omega$  is measured in terms of the tunneling strength,  $t$ , which is the natural energy scale of the system, while  $G(\omega)$  is a pure number. The colors denote different distances to the horizon  $m$ , expressed in lattice sites: blue (lower) is far away and red (taller) is closest to it. (b) Wightman response function of the same system in the frequency domain, measured with respect to the proper time  $\tau = \xi t$ . The proper frequency is  $\omega/\xi$ , while taking the Fourier transform with respect to  $\tau$  requires rescaling  $G(\omega) \rightarrow \xi G(\omega/\xi)$ . As explained in the main text,  $\xi G(\omega/\xi)$  represents what a static De Witt detector in Rindler space-time would observe. Notice that the curves collapse to Fermi-Dirac distributions of increasing temperatures as we approach the horizon. For  $|\omega/\xi| > 1$  lattice artifacts (deviations from the relativistic dispersion relation) distort the response.

As a last step, we study the robustness of our protocol under an increase in the physical temperature of the gas. This results in an imperfect preparation of the Minkowski vacuum, which is the starting point of the protocol. Figure 4(a) compares the rescaled response functions for a 1D system at physical temperature  $T = 0$  and  $\frac{1}{10}$ , measured at two different points, one close to the horizon and one far from it. At  $T = \frac{1}{10}$  the distributions are rounded near  $\omega = 0$ , but we can still see that the one closest to the horizon is more curved and presents a larger probability for positive-energy excitations. The 2D case is more robust, as shown in Fig. 4(b). There, we can see that the rescaled distributions at  $T = 1$  measured near and far from the horizon are clearly distinguished, and keep the same

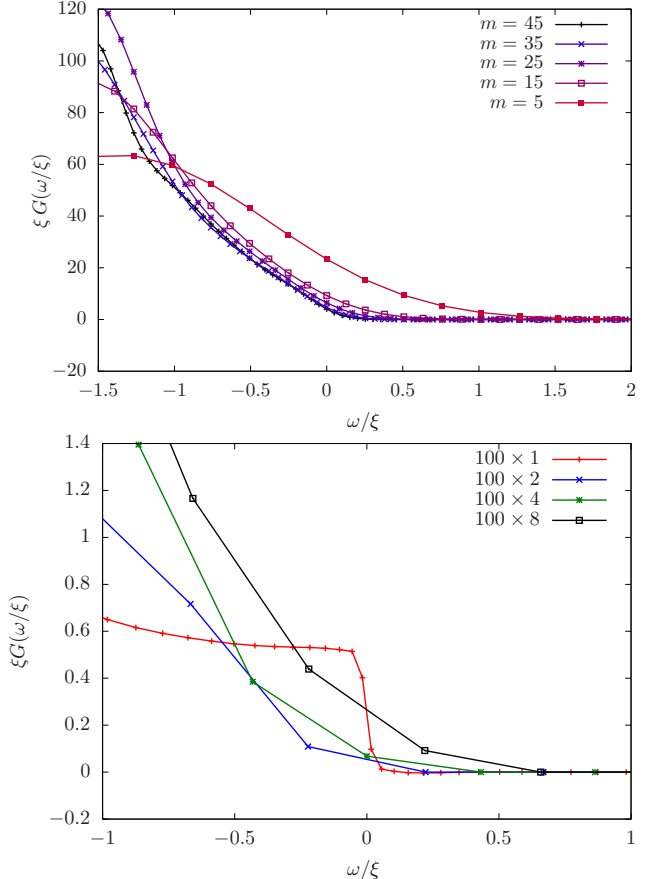


FIG. 3. (a) Wightman response function in the proper frequency domain for a 2D system of size  $100 \times 100$  after the quench. The frequency  $\omega$  is measured in terms of the tunneling strength,  $t$ , which is the natural energy scale of the system, while  $G(\omega)$  is a pure number. As previously, the colors denote different distances to the horizon  $m$  expressed in lattice units: blue (+ signs) is far away, red (full squares) is closest to it. (b) Same for strips of different widths,  $100 \times 1$  to  $100 \times 8$ .

global features than at  $T = 0$ . The explicit expression used to calculate the response functions for a thermal gas is given in the Appendix, Sec. A 3.

## E. Experimental implementation

Our proposal to implement experimentally the Dirac Hamiltonian in Minkowski and Rindler space-times is based on the recent experimental realizations of the Hofstadter model with ultracold atoms [75–77], but in the symmetric gauge and using fermionic atoms instead.

As sketched in Fig. 5, a two-dimensional square lattice with bare tunneling matrix elements  $J$  along the  $x$  and  $y$  directions, and lattice spacing  $d = \lambda_L/2$  (where  $\lambda_L$  is the wavelength of the lattice beams), is subjected to a potential gradient oriented along the diagonal direction of the lattice. This leads to an energy offset between neighboring sites  $\Delta \gg J$  which inhibits tunneling. The offset value could depend on the state of the atom, but should be identical along the  $x$  and  $y$  directions. A pair of Raman laser beams collinear with the lattice beams, of wave vectors  $\mathbf{k}_{1,2}$  and frequencies

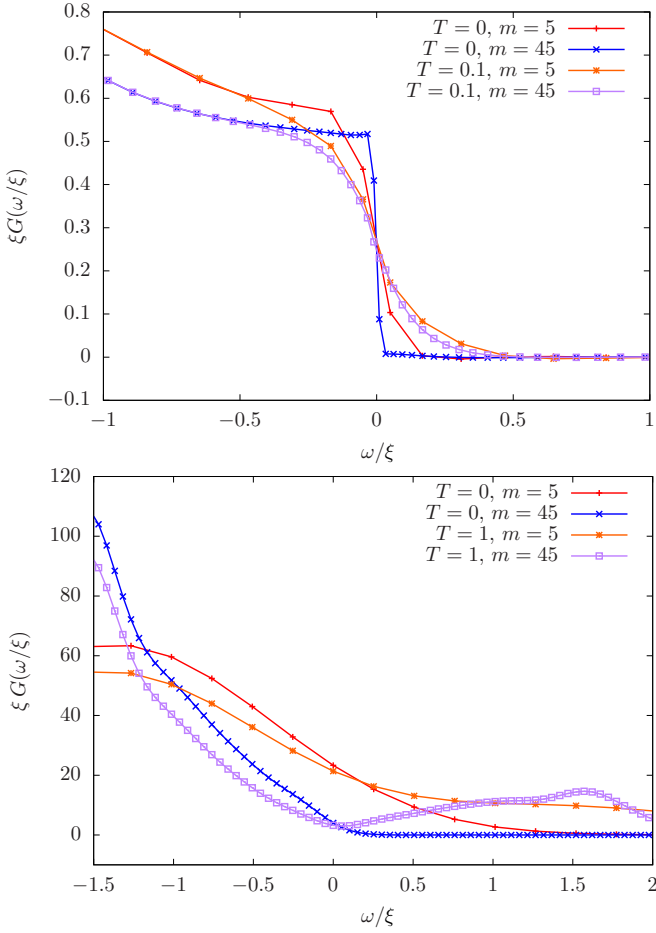


FIG. 4. (a) Comparison between the Wightman response functions in the proper frequency domain for a 1D system of size  $L_x = 100$  after the quench, for two different physical temperatures  $T = 0$  and  $\frac{1}{10}$ , and at two different locations, near and far from the horizon. The frequency  $\omega$  is measured in terms of the tunneling strength,  $t$ , which is the natural energy scale of the system, while  $G(\omega)$  is a pure number. The two response functions at  $T = \frac{1}{10}$  resemble Fermi-Dirac distributions at finite temperature, but the one measured closer to the horizon corresponds to a higher temperature than the one measured far away. (b) Same comparison for a 2D system of size  $100 \times 100$ . The response curves keep their global features when increasing the system temperature from  $T = 0$  to 1. The response function far from the horizon,  $m = 45$ , shows a local maximum at positive frequencies before decaying. This behavior is analogous to the one expected for a thermal gas of Dirac fermions in the homogeneous tunneling lattice (see Appendix, Sec. A 3, Fig. 7). Indeed, in Rindler space-time the limit  $m \rightarrow \infty$  corresponds to zero acceleration and converges to the results of Minkowski space-time.

$\omega_{1,2}$ , result in an additional optical potential

$$V_K(\mathbf{r}) \propto \frac{V_K^0(\mathbf{r})}{2} \cos(\mathbf{q} \cdot \mathbf{r} + \omega t), \quad (35)$$

with  $\mathbf{q} = \mathbf{k}_1 - \mathbf{k}_2$  and  $\omega = \omega_1 - \omega_2$ . The potential amplitude  $V_K^0(\mathbf{r})$  is assumed to be a slowly varying function of  $\mathbf{r}$ . The effect of the Raman beams is to restore tunneling along the two directions when the condition  $\omega = \Delta/\hbar$  is fulfilled, but with a spatial dependence of the phase. In the high-frequency limit  $\hbar\omega \gg J$ , the system is then described by the effective

Hamiltonian

$$H = - \sum_{m,n} \left[ t \left( m + \frac{1}{2}, n \right) e^{i\phi_{m,n}} c_{m+1,n}^\dagger c_{m,n} \right. \\ \left. + t(m,n) e^{i\phi_{m,n}} c_{m,n+1}^\dagger c_{m,n} \right] + \text{H.c.} \quad (36)$$

Here, the phase factor is  $\phi_{m,n} = \mathbf{q} \cdot \mathbf{r} = m\phi_x + n\phi_y$ . The Dirac Hamiltonians (29) and (30) are special cases of (36). For the Raman laser propagation directions displayed in Fig. 5 and a Raman laser wavelength  $\lambda_R = 2\lambda_L$ , the phases are  $\phi_x = -\phi_y = \pi/2$ , which correspond to the  $\pi$ -flux Hamiltonian in the symmetric gauge. The laser-assisted tunneling amplitudes are then given by

$$t(m,n) \simeq t \mathcal{J}_1[V_K^0(m d, n d)/\sqrt{2}\Delta] \\ \simeq t V_K^0(m d, n d)/2\sqrt{2}\Delta, \quad (37)$$

where  $\mathcal{J}_1(x)$  is the Bessel function of the first kind. This expression is valid in the limit  $\Delta \gg V_K^0(m d, n d)$  and for slowly varying  $V_K^0(\mathbf{r})$ , which allows to use as average amplitude of the potential its value at the center of the link. This scheme allows for the simulation of the whole family of optical metrics [41] considered by some of us in [46], and also of extensions of this family to include a mild time dependence in the metric [78].

The realization of the Dirac Hamiltonian in Minkowski space-time requires laser-assisted tunneling amplitudes  $t(m,n) = t_0$  homogeneous across the cloud, which correspond to a constant value of the Raman optical potential amplitude. This could be realized using Gaussian Raman beams of waist  $w_0$  much larger than the cloud size [see Fig. 5(a)]. In order to implement the Dirac Hamiltonian in Rindler space-time, we need instead tunneling amplitudes which increase linearly along the  $x$  direction  $t(m,n) = t'_0 m$  or, equivalently, a Raman optical potential amplitude proportional to  $x$ . Using a  $\text{TEM}_{10}$  Hermite-Gauss mode [79] for the  $y$  Raman beam results in the large beam limit in a Raman optical potential

$$V_K^R(\mathbf{r}) \propto \sqrt{2} \left( \frac{x}{w_0} \right) V_K^0 \cos(\mathbf{q} \cdot \mathbf{r} + \omega t), \quad (38)$$

which, as follows from (37), leads to the required spatial dependence of  $t$  [see Fig. 5(b)]. The quench between the two situations (Minkowski and Rindler) could be performed by a sudden change of the mode of the  $y$  Raman beam, on a time scale of  $\sim 10 \mu\text{s}$ . This is well below the shortest time scale of the system, given by the inverse of the highest tunneling rate, which will typically be on the order of  $\sim 10 \text{ ms}$ . We thus consider the quench as instantaneous. Finally, this scheme can be easily modified, adding for example a superlattice potential along the  $y$  direction, in order to interpolate between the 1D and 2D situations and observe the inversion of statistics.

For measuring the Wightman function  $G(\omega)$ , we propose to perform local spectroscopy of the energy bands and determine their occupation as a function of energy. This information is contained in the transfer rate from an atomic state experiencing the Dirac Hamiltonian in Rindler space-time after the quench, to an auxiliary atomic state with a different dispersion relation. It could thus be measured using one-particle excitation spectroscopy, as demonstrated in [80] and more recently used to

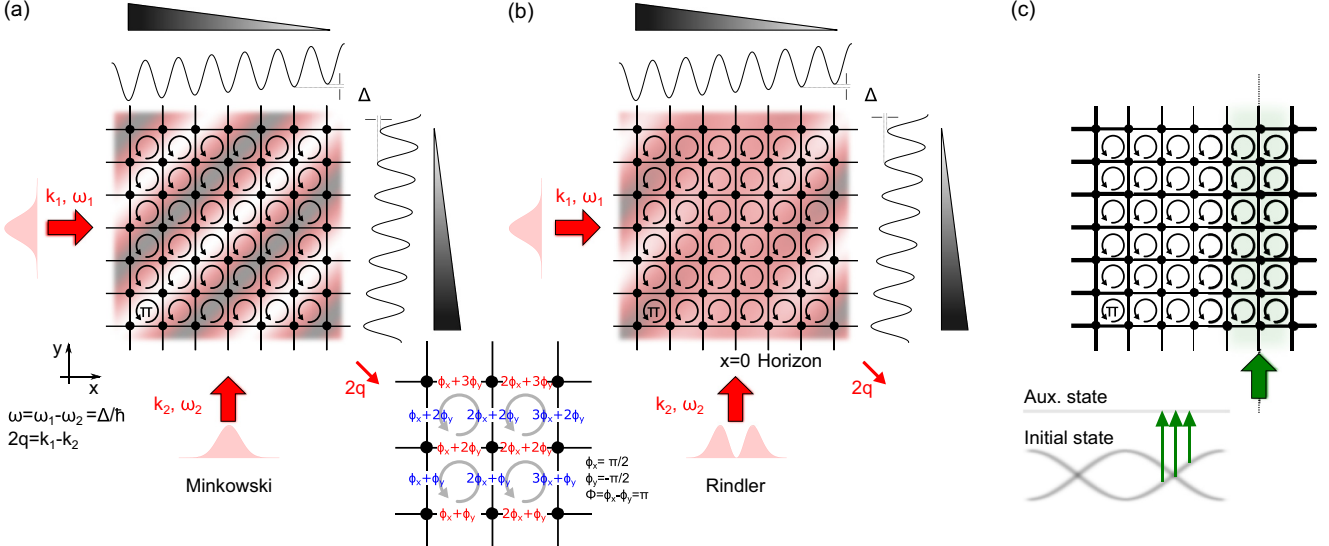


FIG. 5. (a) Experimental scheme for implementing the  $\pi$ -flux model in the symmetric gauge with homogeneous tunneling amplitudes (Minkowski). A linear potential gradient of amplitude  $\Delta$  is superimposed along the diagonal direction of a 2D lattice. Tunneling is restored using a pair of Raman beams of frequencies  $\omega_{1,2}$  and wave vectors  $\mathbf{k}_{1,2}$  which create a modulated potential of frequency  $\omega = \Delta/\hbar$  and wave vector  $\mathbf{q}$  (red snapshot). This leads to complex tunneling with the required spatial dependence of the phase (inset). The tunneling amplitude is homogeneous over the system when using Gaussian Raman beams of large waist compared to the size of the cloud. (b) The Dirac Hamiltonian in Rindler space-time is realized when one of the Raman beams has instead a TEM<sub>10</sub> Hermite-Gauss spatial mode, leading to a linear dependence of the tunneling amplitude with respect to  $x = 0$  (event horizon). (c) The measurement of the detector response function could be realized by local band spectroscopy, using a spectroscopy beam focused at different distances to the horizon (green).

characterize spin-orbit-coupled Fermi gases [81,82]. In order to perform local measurements and determine the dependence of the detector response function with the distance to the horizon, the transfer could be performed using a spectroscopy beam [74] focused at different  $x$  positions [see Fig. 5(c)]. Note that the finite waist of this measurement beam, larger than the lattice spacing, would remove from the measurement some of the discretization artifacts discussed previously, and is equivalent to the convolution procedure used in the numerics (see Appendix, Sec. A 3). Experimentally, the most challenging requirement for this local spectroscopy scheme is to realize  $\pi$ -flux model using an atomic species where one atomic state is subjected to the Dirac Hamiltonian in Minkowski and Rindler space-times, whereas the second (auxiliary) state experiences a different dispersion relation. This situation could be achieved exploiting the ground ( ${}^1S_0$ ) and long-lived metastable excited state ( ${}^3P_0$ ) of the fermionic isotopes of Yb or Sr since the different polarizability of the two states leads to different optical potentials for a broad range of lattice and Raman beam wavelengths  $\lambda_L$  and  $\lambda_R = \frac{2\pi}{k_{1,2}}$ .  $\lambda_L$  would then be chosen such that the auxiliary band has a negligible bandwidth compared to the initial one. In this scheme, the potential gradient leading to the site offset  $\Delta$  should be realized optically as well. The spectroscopy would be performed using a single laser tuned to the clock transition. This ensures an excellent energy resolution, below the tunneling energy scale, as recently demonstrated experimentally in Refs. [83,84].

## V. CONCLUSIONS AND FURTHER WORK

We have developed a proposal for a quantum simulator of the Unruh effect in 1D and 2D massless fermionic fields using

ultracold atoms in an optical lattice. The addition of interacting fields and disorder is possible in our approach, which therefore constitutes a full framework for the study of the theoretical implications of quantum field theory in curved space-time. Moreover, our simulator provides a setting for the study of relativistic quantum information theory in an experimentally accessible system.

The implementation of this quantum simulator is within experimental reach using state-of-the-art experimental techniques. The detection methods proposed here are potentially relevant also for detecting topological properties in simulators of topological insulators and to assess the properties of quantum systems out of equilibrium.

In this work, we have restricted ourselves to the study of the Rindler metric, i.e., Minkowski space-time viewed by an accelerated observer. Nonetheless, the formalism and experimental tools described here may be extended to the study of more complex space-times, for instance, nonstatic or even nonstationary ones. Our work can also be considered as a mandatory step prior to the inclusion of matter back-reaction in the artificial metric, and to the simulation of dynamical gravity fields. Thus, this work paves the way to experiments that are not only fascinating *per se*, but are also able to access phenomena that are not fully understood theoretically, such as gravitating quantum matter in interaction.

Finally, the recent conceptual developments towards a combination of quantum mechanics and general relativity, such as quantum graphity [85,86] or the Maldacena-Susskind notion of relating entanglement and space-time in order to avoid the firewall problem [87], might also be amenable to quantum simulation using a similar approach.

## ACKNOWLEDGMENTS

This work has been supported by Spanish MINECO (SEVERO OCHOA Grants No. SEV-2015-0522, No. FOCUS FIS2013-46768, No. FIS2014-59546-P, No. FIS2012-33642, No. FISICATEAMO FIS2016-79508-P, and No. RyC-2015-17890), Agència de Gestió d'Ajuts Universitaris i de Recerca (2014SGR874), Fundació Cellex, DFG (FOR2414) and EU grants EQuaM (FP7/2007-2013 Grant No. 323714), OSYRIS (ERC-2013-AdG Grant No. 339106), SIQS (FP7-ICT-2011-9 Grant No. 600645), QUIC (H2020-FETPROACT-2014 Grant No. 641122) and Grant No. PCIG13-GA-2013-631633. The authors want to acknowledge A. Enciso, I. Fuentes, J. Korbicz, J. León, D. Peralta, C. Sabín, and G. Sierra for very fruitful discussions.

## APPENDIX: EIGENSTATES OF THE RINDLER HAMILTONIAN IN 1D

Let us restrict ourselves to 1D. Since the  $x < 0$  and  $x > 0$  regions are effectively separated, we may restrict ourselves to the right half-line. Consider the spinless 1D version of Eq. (27),  $H_{R(1D)} = \sqrt{x} p \sqrt{x}$ . Notice that  $x \partial_x = \partial_{\ln(x)}$ . Let us define  $u \equiv \ln(x)$ , taking the horizon to  $-\infty$ . So,  $H_{R(1D)} = -i(\partial_u + 1/2)$ . The eigenvalue equation is

$$-i(x \partial_x + 1/2)\psi(x) = -i(\partial_u + 1/2)\psi(u) = \omega\psi(u). \quad (\text{A1})$$

The solutions to that equation have the form

$$\psi(u) = A \exp\left[(i\omega - \frac{1}{2})u\right] = A x^{i\omega-1/2}, \quad (\text{A2})$$

so they are plane waves in  $u = \ln(x)$ . Figure 6 shows the behavior of these wave functions.

In order to ensure that the Hamiltonian is truly Hermitian, we can check that the eigenfunctions corresponding to different eigenvalues are orthogonal. Indeed, they are

$$\begin{aligned} \int_0^\infty dx \exp[-i\omega - 1/2)u] \exp[i\omega' - 1/2)u] \\ = \int_{-\infty}^\infty du \exp(-i\omega u) \exp(i\omega' u) = \delta(\omega - \omega'). \end{aligned} \quad (\text{A3})$$

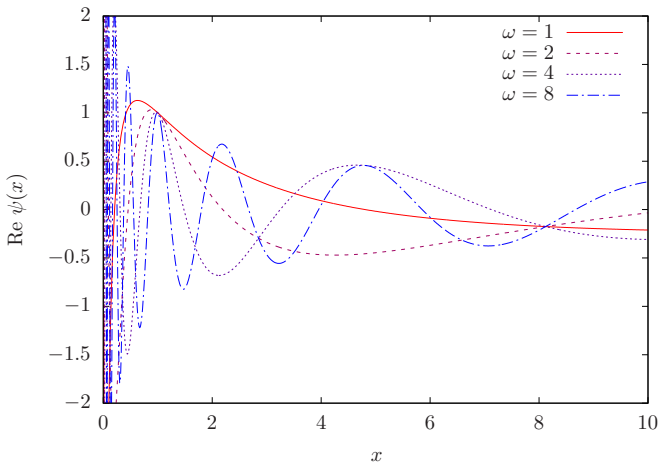


FIG. 6. One-dimensional Rindler modes [Eq. (A2)] for different values of  $\omega$ . Both  $x$  and  $\omega$  are measured in arbitrary units of length and frequency, respectively.

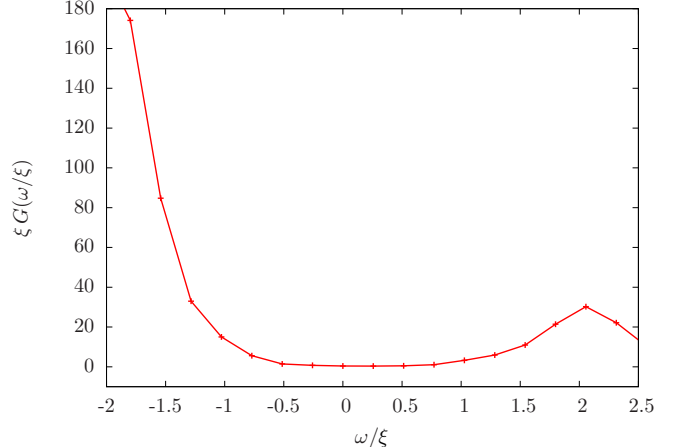


FIG. 7. Wightman response function for a 2D thermal gas of Dirac fermions in Minkowski space. The frequency  $\omega$  is measured in terms of the tunneling strength,  $t$ , which is the natural energy scale of the system, while  $G(\omega)$  is a pure number. As expected from the behavior of the density of states of the 2D Fermi gas in a  $\pi$ -flux lattice, the response has a maximum at positive frequency  $\omega$ . The response above coincides with the one obtained in Rindler space-time in Fig. 4 at very large distance from the horizon.

Let us insert the spinor structure. For  $x > 0$ ,

$$-i(x \partial_x + 1/2)\sigma_x \begin{pmatrix} \psi_1 \\ \psi_2 \end{pmatrix} = \omega \begin{pmatrix} \psi_1 \\ \psi_2 \end{pmatrix}, \quad (\text{A4})$$

which leads to  $(\partial_u + 1/2)^2 \psi_1 = -\omega^2 \psi_1$ , and an equivalent equation for  $\psi_2$ . The solution is very similar to the nonspinorial case

$$\begin{pmatrix} \psi_1(x,t) \\ \psi_2(x,t) \end{pmatrix} = A \begin{pmatrix} 1 \\ \pm 1 \end{pmatrix} x^{i\omega-1/2} e^{-i\omega t}. \quad (\text{A5})$$

## 1. Discretization of the Rindler Hamiltonian

The implementation of an analog of equations (19) or (27) in an optical lattice requires a suitable discretization. In this section, we will discuss the 1D case.

Let us discuss how to discretize  $H_{R(1D)} = \sqrt{x} p \sqrt{x}$ , the 1D Rindler Hamiltonian, appropriately. Consider an open 1D lattice with spacing  $d$ , and lattice points  $x_m = md$ , with  $m \in \{-(L-1)/2, \dots, (L-1)/2\}$  and even  $L$ . Thus, the wave functions only take components  $\psi_m \equiv \psi(x_m)$ . Let us use a central differences discretization for  $p = -i\partial_x$ , i.e.,  $(p\psi)_m = -i(\psi_{m+1} - \psi_{m-1})/(2d)$ . Let us call  $R$  the discrete version of the  $H_{R(1D)}$ , for later convenience:

$$\begin{aligned} (R\psi)_m &= \sqrt{x_m}(p\sqrt{x}\psi)_m \\ &= -\frac{i}{2}[\sqrt{m(m+1)}\psi_{m+1} - \sqrt{m(m-1)}\psi_{m-1}] \\ &= \sum_{m'} R_{m,m'} \psi_{m'}. \end{aligned} \quad (\text{A6})$$

Thus, the matrix entries for the Hamiltonian  $R_{m,m'}$  are nonzero only when the difference between the spatial indices

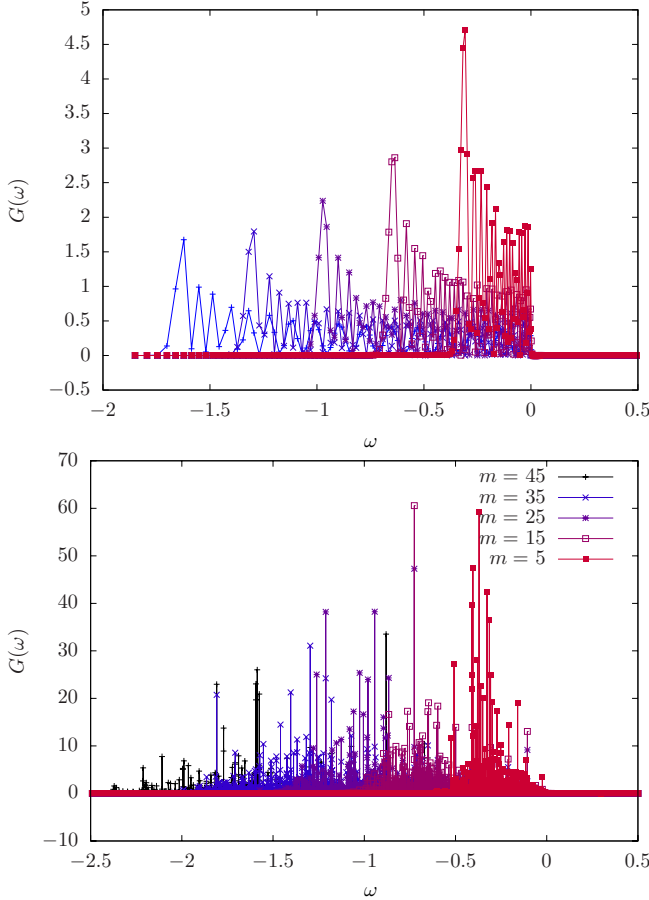


FIG. 8. (a) Raw response function in the frequency domain for a 1D system prior to Gaussian convolution as in (A17). The frequency  $\omega$  is measured in terms of the tunneling strength,  $t$ , which is the natural energy scale of the system, while  $G(\omega)$  is a pure number. The system size is  $L_x = 500$ , and the color (and point type) denoting the distance to the horizon are the same as in Fig. 2(a). (b) Raw response function in the frequency domain for a 2D system prior to Gaussian convolution as in (A17) and the frequency rescaling described in Sec. IV C. The system size,  $L_x = 500$ , and the color code (and point type) denoting the distance to the horizon are the same as in Fig. 3(a).

is one:  $|m - m'| = 1$ . In that case,

$$R_{m,m+1} = -\frac{i}{2} \sqrt{m(m+1)}. \quad (\text{A7})$$

This means that the tunneling between sites  $m$  and  $m + 1$  must be  $-(i/2) \sqrt{m(m+1)}$ , independently of  $d$ . This is not surprising since both  $R$  and Rindler space-time are *scale invariant*. A good approximation is obtained by replacing the *geometric mean* by the *arithmetic mean*:  $R_{m,m+1} \approx -(i/2)(m + 1/2)$ .

The discrete Hamiltonian (A7) can be analytically diagonalized [51]. Its spectrum becomes continuous with constant energy level density as  $L \rightarrow \infty$ , but the convergence rate is very slow: the distance between levels scales as  $\approx 1/\ln(L)$ .

Let us now focus on the 2D case. In order to formulate the Rindler Hamiltonian on a square lattice it is convenient to start with the symmetric continuous formulation (26). Explicitly, by writing the spinor in terms of its chiral components,

$\psi(x,y) = (a^{(x,y)}_b, b^{(x,y)}_b)$ , we have

$$H_R = \frac{i}{2} \int dx dy |x| [\partial_x a^\dagger(x,y) - i \partial_y a^\dagger(x,y)] b(x,y) + \text{H.c.} \quad (\text{A8})$$

We can now exploit the bipartition of the lattice for discretizing separately the two chiralities in the two checkerboard sublattices and write the kinetic term in terms of the tunneling between the two:

$$\begin{aligned} H_R = \frac{i}{4} t'_0 \sum_{k,l} & \left( |k+l+\frac{1}{2}| a_{k+l+1,k-l}^\dagger \right. \\ & - |k+l-\frac{1}{2}| a_{k+l-1,k-l}^\dagger - i |k+l| a_{k+l,k-l+1}^\dagger \\ & \left. + i |k+l| a_{k+l,k-l-1}^\dagger \right) b_{k+l,k-l} + \text{H.c.} \end{aligned} \quad (\text{A9})$$

At this point, we notice that the above Hamiltonian can be rewritten as the  $\pi$ -flux Hamiltonian once we do not distinguish fermions in the different sublattices. Denoting the annihilation (creation) operators by  $c_{m,n}$  ( $c_{m,n}^\dagger$ ),

$$\begin{aligned} H_R = \frac{t'_0}{2} \sum_{m,n} & \left[ i |m+\frac{1}{2}| c_{m+1,n}^\dagger + (-1)^{m+n} |m| c_{m,n+1}^\dagger \right] c_{m,n} \\ & + \text{H.c.} \end{aligned} \quad (\text{A10})$$

By applying the gauge transformation

$$c_{m,n}^\dagger \rightarrow e^{i \frac{\pi}{4} (m^2 - 4n^2 - 2mn - 3m + 4n)} c_{m,n}^\dagger, \quad (\text{A11})$$

we can recover the  $\pi$ -flux Hamiltonian in the symmetric gauge (30).

## 2. Relation to the Riemann conjecture

The Dirac Hamiltonian is of interest in very different areas, not only of physics, but also of mathematics. Indeed, fermionic models are regularly used as mathematical tools in differential geometry and analytic number theory. For instance, by studying the number of nontrivial solutions of a Dirac operator in a given manifold, it is possible to determine the topological properties of the manifold itself as proved by the celebrated Atiyah-Patodi-Singer index theorem [88].

The Dirac Hamiltonian in Rindler space-time considered in this paper and its nonspinorial 1D equivalent  $H = \sqrt{x} p \sqrt{x}$  provide a handle for proving the Riemann conjecture, which is one of the most famous and relevant open problems in mathematics. Riemann conjectured that the nontrivial zeros of the Riemann zeta function  $\zeta(s)$  in the complex plane all have real part  $\frac{1}{2}$  [89]. One of the established routes towards proving this conjecture, the Hilbert-Polya route, is especially interesting for physicists as it attempts the construction of a Hermitian operator whose eigenvalues are the imaginary parts of the nontrivial Riemann zeros. In physics, natural occurrences of Hermitian operators are, of course, quantum Hamiltonians [50]. In 1999, Berry and Keating proposed the  $H = xp$  Hamiltonian and showed how the statistical behavior of its eigenvalues corresponded to the statistical average behavior of the imaginary parts of the nontrivial Riemann zeros [90]. In fact, the classical Hamiltonian  $H = xp$  must

be supplemented with a quantization prescription. The most natural one is

$$H = \sqrt{x} p \sqrt{x} = -i(\sqrt{x} \partial_x \sqrt{x}) = -i(x \partial_x + 1/2), \quad (\text{A12})$$

i.e., the 1D version of the Dirac Hamiltonian in Rindler space-time. The discovery of this Berry-Keating Hamiltonian led to a series of attempts to extend the model in several directions [51,52], including a recent spinorial extension, which is Eq. (27) [53].

### 3. Response function for a thermal gas and Gaussian convolution

In Sec. II C, we have derived the expression for the Wightman response function in the frequency domain  $G(\omega)$  for the ideal case of fermionic atoms at zero temperature [Eq. (16)]. For a realistic gas at finite temperature  $T$  considered at the end of Sec. IV C, the Minkowski vacuum  $|0_M\rangle$ , appearing in (16), has to be replaced by the thermal mixed state  $\rho_M(T)$ :

$$\rho_M(T) = \sum_k \frac{1}{1 + \exp[\hbar\omega_k^M/k_B T]} b_k^\dagger |\Omega\rangle\langle\Omega| b_k. \quad (\text{A13})$$

It follows that the response function for a thermal gas is

$$\begin{aligned} G_{x_0}(\omega) &= \text{Tr}[\rho_M(T)c_{x_0}^\dagger c_{x_0}] \\ &= \sum_{q,q'} \delta(\omega - \omega_q^R) \bar{R}_{q,x_0} R_{q'x_0} C_{qq'}, \end{aligned} \quad (\text{A14})$$

where

$$C_{qq'} = \sum_k \bar{U}_{qk} U_{q'k} \frac{1}{1 + \exp[\hbar\omega_k^M/k_B T]}. \quad (\text{A15})$$

Note that for  $T \rightarrow 0$ ,  $C_{qq'} \rightarrow \sum_{\omega_k^M < 0} \bar{U}_{qk} U_{q'k}$ , and one recovers the zero-temperature response function (16). For  $T$  larger of  $T_U$ , the response function becomes identical to the one of an ordinary thermal Fermi gas in Minkowski spacetime, shown in Fig. 7. As defined in the main text, Eqs. (11) and (15), the unitary matrices  $U_{qk}$  and  $R_{qx}$  are determined from the single-particle modes of Dirac Hamiltonian in Minkowski and Rindler space-time.

In Sec. II C, in order to smear out lattice artifacts, we have considered a convolution of the response function with a Gaussian. In fact, as explained in Sec. IV E, such convolution is what is really detected by one-particle excitation spectroscopy. The Gaussian convolution consists of the following. By defining

$$F(x - x_0) = \frac{1}{\sqrt{2\pi}\sigma} \exp[-(x - x_0)^2/2\sigma^2], \quad (\text{A16})$$

the convoluted response function reads as

$$G_{x_0}^F(\omega) = \sum_{q,q'} \delta(\omega - \omega_q^R) \sum_x F(x - x_0) \bar{R}_{q,x} R_{q'x} C_{qq'}, \quad (\text{A17})$$

where  $x$ 's are the abscissas of the lattice sites  $x = m$  (the lattice space is taken to be one for convenience). The response functions presented in Figs. 2–4 are obtained by taking  $\sigma = 2$ . The raw data are shown in Fig. 8.

- 
- [1] N. Birrell and P. Davies, *Quantum Fields in Curved Space* (Cambridge University Press, Cambridge, 1982).
- [2] J. D. Bekenstein, *Phys. Rev. D* **7**, 2333 (1973).
- [3] S. W. Hawking, *Commun. Math. Phys.* **43**, 199 (1975).
- [4] S. A. Fulling, *Phys. Rev. D* **7**, 2850 (1973).
- [5] P. C. W. Davies, *J. Phys. A: Math. Gen.* **8**, 609 (1975).
- [6] W. G. Unruh, *Phys. Rev. D* **14**, 870 (1976).
- [7] S. Takagi, *Prog. Theor. Phys. Suppl.* **88**, 1 (1986).
- [8] L. Susskind and J. Lindesay, *An Introduction to Black Holes, Information and the String Theory Revolution* (World Scientific, Singapore, 2005).
- [9] T. Jacobson, *Phys. Rev. Lett.* **75**, 1260 (1995).
- [10] D. Singleton and S. Wilburn, *Phys. Rev. Lett.* **107**, 081102 (2011).
- [11] P. D. Nation, J. R. Johansson, M. P. Blencowe, and F. Nori, *Rev. Mod. Phys.* **84**, 1 (2012).
- [12] P. C. W. Davies and S. A. Fulling, *Proc. R. Soc. London* **356**, 237 (1977).
- [13] A. Calogeracos, *J. Phys. A: Math. Gen.* **35**, 3415 (2002).
- [14] A. Calogeracos, *J. Phys. A: Math. Gen.* **35**, 3435 (2002).
- [15] J. G. Russo and P. K. Townsend, *Class. Quantum Grav.* **25**, 175017 (2008).
- [16] M. Chernicoff and A. Paredes, *J. High Energy Phys.* **03** (2011) 063.
- [17] L. C. B. Crispino, A. Higuchi, and G. E. A. Matsas, *Rev. Mod. Phys.* **80**, 787 (2008).
- [18] E. Martín-Martínez, I. Fuentes, and R. B. Mann, *Phys. Rev. Lett.* **107**, 131301 (2011).
- [19] C. Barceló, S. Liberati, and M. Visser, *Living Rev. Relativity* **8**, 12 (2005).
- [20] G. Volovik, *The Universe in a Helium Droplet* (Oxford University Press, Oxford, 2003).
- [21] W. G. Unruh, *Phys. Rev. Lett.* **46**, 1351 (1981).
- [22] S. Weinfurtner, E. W. Tedford, M. C. J. Penrice, W. G. Unruh, and G. A. Lawrence, *Phys. Rev. Lett.* **106**, 021302 (2011).
- [23] S. Weinfurtner, E. W. Tedford, M. C. J. Penrice, W. G. Unruh, and G. A. Lawrence, *Analogue Gravity Phenomenology* (Springer, Berlin, 2013).
- [24] L. J. Garay, J. R. Anglin, J. I. Cirac, and P. Zoller, *Phys. Rev. A* **63**, 023611 (2001).
- [25] P. O. Fedichev and U. R. Fischer, *Phys. Rev. Lett.* **91**, 240407 (2003).
- [26] P. O. Fedichev and U. R. Fischer, *Phys. Rev. D* **69**, 064021 (2004).
- [27] J. Steinhauer, *Nat. Phys.* **10**, 864 (2014).
- [28] J. Steinhauer, *Nat. Phys.* **12**, 959 (2016).
- [29] P. O. Fedichev and U. R. Fischer, *Phys. Rev. A* **69**, 033602 (2004).

- [30] I. Carusotto, R. Balbinot, A. Fabbri, and A. Recati, *Eur. Phys. J. D* **56**, 391 (2010).
- [31] J.-C. Jaskula, G. B. Partridge, M. Bonneau, R. Lopes, J. Ruaudel, D. Boiron, and C. I. Westbrook, *Phys. Rev. Lett.* **109**, 220401 (2012).
- [32] D. Boiron, A. Fabbri, P.-É. Larré, N. Pavloff, C. I. Westbrook, and P. Ziň, *Phys. Rev. Lett.* **115**, 025301 (2015).
- [33] A. Retzker, J. I. Cirac, M. B. Plenio, and B. Reznik, *Phys. Rev. Lett.* **101**, 110402 (2008).
- [34] J. Marino, A. Recati, and I. Carusotto, [arXiv:1605.07642](https://arxiv.org/abs/1605.07642).
- [35] T. G. Philbin, C. Kuklewicz, S. Robertson, S. Hill, F. König, and U. Leonhardt, *Science* **319**, 1367 (2008).
- [36] F. Belgiorno, S. L. Cacciatori, M. Clerici, V. Gorini, G. Ortenzi, L. Rizzi, E. Rubino, V. G. Sala, and D. Faccio, *Phys. Rev. Lett.* **105**, 203901 (2010).
- [37] R. Schützhold and W. G. Unruh, *Phys. Rev. Lett.* **107**, 149401 (2011).
- [38] W. G. Unruh and R. Schützhold, *Phys. Rev. D* **86**, 064006 (2012).
- [39] S. Finazzi and I. Carusotto, *Phys. Rev. A* **89**, 053807 (2014).
- [40] A. Iorio and G. Lambiase, *Phys. Lett. B* **716**, 334 (2012).
- [41] M. Cvetic and G. W. Gibbons, *Ann. Phys. (NY)* **327**, 2617 (2012).
- [42] A. Iorio and G. Lambiase, *Phys. Rev. D* **90**, 025006 (2014).
- [43] C. M. Wilson, G. Johansson, A. Pourkabirian, M. Simoen, J. R. Johansson, T. Duty, F. Nori, and P. Delsing, *Nature (London)* **479**, 376 (2011).
- [44] L. Tarruell, D. Greif, T. Uehlinger, G. Jotzu, and T. Esslinger, *Nature (London)* **483**, 302 (2012).
- [45] M. Lewenstein, A. Sanpera, and V. Ahufinger, *Ultracold Atoms in Optical Lattices* (Oxford University Press, Oxford, 2012).
- [46] O. Boada, A. Celi, J. I. Latorre, and M. Lewenstein, *New J. Phys.* **13**, 035002 (2011).
- [47] I. Bloch, J. Dalibard, and W. Zwerger, *Rev. Mod. Phys.* **80**, 885 (2008).
- [48] P. M. Alsing and I. Fuentes, *Class. Quantum Grav.* **29**, 224001 (2012).
- [49] M. Asorey, A. Ibort, and G. Marmo, *Int. J. Mod. Phys. A* **20**, 1001 (2005).
- [50] D. Schumayer and D. A. W. Hutchinson, *Rev. Mod. Phys.* **83**, 307 (2011).
- [51] G. Sierra, *J. Stat. Mech.* (2005) P12006.
- [52] G. Sierra and J. Rodríguez-Laguna, *Phys. Rev. Lett.* **106**, 200201 (2011).
- [53] K. S. Gupta, E. Harikumar, and A. R. de Queiroz, *Europhys. Lett.* **102**, 10006 (2013).
- [54] H. Ueda and T. Nishino, *J. Phys. Soc. Jpn.* **78**, 014001 (2009).
- [55] M. Vekić and S. R. White, *Phys. Rev. Lett.* **71**, 4283 (1993).
- [56] V. G. Rousseau, G. G. Batrouni, D. E. Sheehy, J. Moreno, and M. Jarrell, *Phys. Rev. Lett.* **104**, 167201 (2010).
- [57] C. W. Misner, K. S. Thorne, and J. A. Wheeler, *Gravitation* (W. H. Freeman, San Francisco, 1973).
- [58] R. M. Wald, *General Relativity* (University of Chicago Press, Chicago, 1984).
- [59] R. Sachs and H. Wu, *General Relativity for Mathematicians* (Springer, Berlin, 1983).
- [60] R. C. Tolman and P. Ehrenfest, *Phys. Rev.* **36**, 1791 (1930).
- [61] H. Li and F. D. M. Haldane, *Phys. Rev. Lett.* **101**, 010504 (2008).
- [62] I. Peschel, *J. Phys. A: Math. Gen.* **36**, L205 (2003).
- [63] P. Candelas and D. W. Sciama, *Phys. Rev. Lett.* **38**, 1372 (1977).
- [64] P. Candelas and D. Deutsch, *Proc. R. Soc. London, Ser. A* **354**, 79 (1977).
- [65] R. M. Reed and B. Simon, *Methods of Modern Mathematical Physics II* (Academic, New York, 1975).
- [66] J. Kogut and L. Susskind, *Phys. Rev. D* **11**, 395 (1975).
- [67] I. Affleck and J. B. Marston, *Phys. Rev. B* **37**, 3774 (1988).
- [68] L.-K. Lim, A. Lazarides, A. Hemmerich, and C. Morais Smith, *Europhys. Lett.* **88**, 36001 (2009).
- [69] T. Salger, C. Grossert, S. Kling, and M. Weitz, *Phys. Rev. Lett.* **107**, 240401 (2011).
- [70] P. Soltan-Panahi *et al.*, *Nat. Phys.* **7**, 434 (2011).
- [71] L. Duca, T. Li, M. Reitter, I. Bloch, M. Schleier-Smith, and U. Schneider, *Science* **347**, 288 (2015).
- [72] M. Polini, F. Guinea, M. Lewenstein, H. C. Manoharan, and V. Pellegrini, *Nat. Nanotechnol.* **8**, 625 (2013).
- [73] T. Jacqmin, I. Carusotto, I. Sagnes, M. Abbarchi, D. D. Solnyshkov, G. Malpuech, E. Galopin, A. Lemaître, J. Bloch, and A. Amo, *Phys. Rev. Lett.* **112**, 116402 (2014).
- [74] T.-L. Dao, A. Georges, J. Dalibard, C. Salomon, and I. Carusotto, *Phys. Rev. Lett.* **98**, 240402 (2007).
- [75] M. Aidelsburger, M. Atala, M. Lohse, J. T. Barreiro, B. Paredes, and I. Bloch, *Phys. Rev. Lett.* **111**, 185301 (2013).
- [76] H. Miyake, G. A. Siviloglou, C. J. Kennedy, W. C. Burton, and W. Ketterle, *Phys. Rev. Lett.* **111**, 185302 (2013).
- [77] C. J. Kennedy, W. C. Burton, W. C. Chung, and W. Ketterle, *Nat. Phys.* **11**, 859 (2015).
- [78] J. Minář and B. Grémaud, *J. Phys. A: Math. Theor.* **48**, 165001 (2015).
- [79] The required TEM<sub>10</sub> Hermite-Gauss mode could be obtained using a phase plate, a spatial light modulator, or an optical cavity.
- [80] J. T. Stewart, J. P. Gaebler, and D. S. Jin, *Nature (London)* **454**, 744 (2008).
- [81] P. Wang, Z.-Q. Yu, Z. Fu, J. Miao, L. Huang, S. Chai, H. Zhai, and J. Zhang, *Phys. Rev. Lett.* **109**, 095301 (2012).
- [82] L. W. Cheuk, A. T. Sommer, Z. Hadzibabic, T. Yefsah, W. S. Bakr, and M. W. Zwierlein, *Phys. Rev. Lett.* **109**, 095302 (2012).
- [83] S. Kolkowitz, S. L. Bromley, T. Bothwell, M. L. Wall, G. E. Marti, A. P. Koller, X. Zhang, A. M. Rey, and J. Ye, [arXiv:1608.03854](https://arxiv.org/abs/1608.03854); *Nature* (2016), doi:10.1038/nature20811.
- [84] L. F. Livi, G. Cappellini, M. Diem, L. Franchi, C. Clivati, M. Frittelli, F. Levi, D. Calonico, J. Catani, M. Inguscio, and L. Fallani, *Phys. Rev. Lett.* **117**, 220401 (2016).
- [85] A. Hamma, F. Markopoulou, S. Lloyd, F. Caravelli, S. Severini, and K. Markström, *Phys. Rev. D* **81**, 104032 (2010).
- [86] F. Caravelli, F. Markopoulou, A. Riera, and L. Sindoni, [arXiv:1212.1981](https://arxiv.org/abs/1212.1981).
- [87] J. Maldacena and L. Susskind, *Fortschr. Phys.* **61**, 781 (2013).
- [88] R. B. Melrose, *The Atiyah-Patodi-Singer Index Theorem*, Vol. 4 (A K Peters, Wellesley, MA, 1993).
- [89] H. M. Edwards, *Riemann's Zeta Function* (Academic, New York, 1974).
- [90] M. V. Berry and J. P. Keating, *SIAM Rev.* **41**, 236 (1999).